Macromolecules

pubs.acs.org/Macromolecules

Article

Tuning Knotted Copolyelectrolyte Conformations via Solution Properties

Andrea Tagliabue, Cristian Micheletti,* and Massimo Mella*

Cite This: *Macromolecules* 2022, 55, 10761−10772

Read Online

ACCESS | Metrics & More | Article Recommendations | Supporting Information

ABSTRACT: We used Langevin dynamics simulations to study coarse-grained knotted copolyelectrolytes, composed by a neutral and a charged segment, in solutions of different salt concentrations, valency, and solvent screening power. We show that the facile variation of these parameters allows for tuning the length and position of the knotted region, which in turn controls the overall metric properties. Specifically, adding either monovalent or divalent ions causes the knot to swell at the expense of the copolyelectrolyte overall size. However, the knot typically straddles the charged−neutral interface in the presence of monovalent counterions, whereas it is attracted on the charged segment with divalent ones. Notably, similar modulations of knot size and position can also be achieved by varying the dielectric constant of the solvent. Our results demonstrate the feasibility of harnessing the solution-mediated balance of electrostatics and conformational entropy toward a facile external tuning of the conformational properties of knotted polymers.

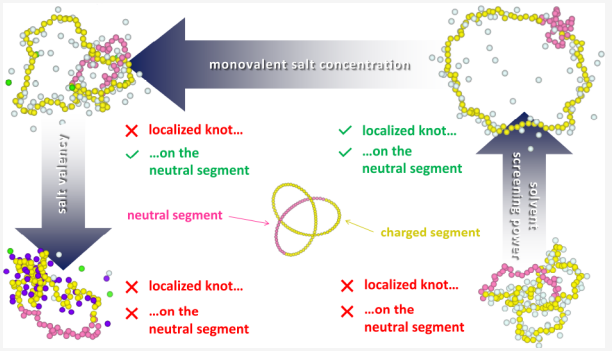

INTRODUCTION

Knots are ubiquitous in naturally occurring polymers such as DNA[1−7] and proteins[8−12] and are increasingly used to design new synthetic molecules and materials.[13−15]

The interest in molecular knots, and their design, is fueled by the increasing evidence that topological constraints can dramatically affect an impressive range of static and dynamic polymer properties, including metric scaling behavior,[16−21] relaxation kinetics,[5,22−29] and the response to external perturbations such as mechanical stretching,[30−33] extensional flows,[34−39] and pore translocation.[40−42] It is thus natural to ask whether there are polymeric systems that allow for a facile design or tuning of their topological constraints, such as their tightness, as this would yield an indirect control over the above-mentioned physical properties.

In this regard, knotted circular copolyelectrolytes (coPE's), i.e., ring polymers featuring charged and neutral blocks, appear uniquely tunable.[43] In fact, varying the coPE composition, hence the (relative) length of the blocks, allows for biasing in specific ways the contour length and position of the knot, thus modulating the coPE size and its internal dynamics. Such effects have no analogue in homopolymers or block copolymers with, e.g., regions of different rigidity.[44]

The unique tunability of coPE's arises from competing contributions to the system Helmholtz (free) energy, namely, (i) the electrostatic repulsion between charged monomers, particularly those kept in proximity by the essential crossings of the knot, (ii) the conformational entropy of the knotted region and, consequently, of the knot complementary arc, and (iii) the entropy of counterions, whose degree of condensation on a knotted polyelectrolyte depends on the latter conformation.[45] Segregating the knot in the neutral block can thus lower the intrachain electrostatic repulsion but only at the expense of the coPE conformational entropy. Accordingly, with judicious choices of the length of the ring polymer[30] and of the neutral segment, one can balance the two terms for desired effects on statics and dynamics.[43]

To achieve the highest level of tunability, one should single out polymer systems where knot length and position depend not only on intrinsic properties like the polymer chemical composition, which is not easily modifiable, but especially on more easily tunable extrinsic ones. Block coPE's are promising candidates also in this respect, as their electrostatic interactions respond to solution properties that can be controlled externally, such as the background ionic strength or the solvent intrinsic screening power (i.e., its dielectric permittivity). For instance, increasing the concentration of salt ions generally reduces the average gyration radius of polyelectrolytes, including strong[46] and weak[45] knotted ones. Interestingly, divalent counterions can much enhance the

Received: September 19, 2022
Revised: November 16, 2022
Published: December 2, 2022

https://doi.org/10.1021/acs.macromol.2c01933
Macromolecules 2022, 55, 10761−10772

effect[45,46] by coordinating several charged monomers, inducing polyelectrolytes compaction.[45,47−54] Changing the solvent screening power (practically, its Bjerrum length l_B), which modulates the strength of the electrostatic potential, can elicit similar effects.[45] In fact, increasing l_B typically augments counterion condensation along the chain contour of weak polyacids, resulting in larger knots. Conversely, tighter knots are obtained by decreasing l_B. In the end, all these considerations motivated the present systematic study of how knotted coPE's respond to changes in ionic strength, counterion valency, and l_B, which can all be experimentally varied in a facile manner.

In the present work, Langevin dynamics simulations and coarse-grained models of knotted coPE's[43,45] are employed to gain more insights into the possibility to exploit the above-mentioned solution properties to tune the conformational and thermodynamical behavior of knotted coPE's. Among our main findings, we first mention that increasing the concentration of monovalent salt yields a longer knot that straddles the neutral segment, thus reducing the overall chain size, across all considered coPE compositions. Differently, adding divalent counterions makes the knot longer while concurrently displacing it from the neutral block. We also show that analogous effects can be achieved by lowering the solvent screening power, whereas its increase promotes a higher overlap between the knot and the neutral segment.

Our results provide a first demonstration of the feasibility of tuning the contour size and position of knots in polymer systems via the facile modification of external parameters; the former characteristics may thus be easily directed toward the desired overall metric properties.

MODEL AND METHODS

Model. The simulated system consists of a single circular knotted copolyelectrolyte (coPE, or "ring") in a periodically repeated cubic cell, whose side length $L = 76.36\sigma$ ($\sigma = 3.55$ Å) was chosen to yield a molar concentration of monomers equal to $C_{mono} = 10^{-2}$ M.

The circular coPE, which has a 3_1 (trefoil) knot topology, is represented via a coarse-grained "beads−springs" primitive model and consists of $N_{mono} = 120$ monomers. The ring includes a segment of N_{neu} adjacent neutral monomers (neutral segment, NS), whereas the remaining $N_{chrg} = N_{mono} - N_{neu}$ ones carry a quenched monovalent negative charge; i.e., they act as strong electrolytes.

Bonds between consecutive beads are modeled via a finitely extensible nonlinear elastic (FENE) potential[55]

$$U_{bond}(r_{ij}) = -\frac{1}{2}k_{bond}r_{max}^{\ 2}\ln\left(1 - \left(\frac{r_{ij}}{r_{max}}\right)^2\right) \quad (1)$$

where r_{ij} is the distance between two bonded monomers i and j, $r_{max} = 3\sigma$ is the maximum allowed bond elongation, and $k_{bond} = 30\epsilon/\sigma^2$ is the force constant. In the latter expression, ϵ is taken equal to the characteristic thermal energy of the system, which is in canonical equilibrium at temperature T, $\epsilon = k_BT$.

In the simulation cell, $N_{CI} = N_{chrg}$ monovalent positive CI's, which are necessary to counterbalance the negative charge carried by the polyelectrolyte, and N_s symmetric (i.e., z:z) salt pairs, either monovalent ($z = 1$) or divalent ($z = 2$), are also present.

All particles (i.e., monomers and ions in solution) are treated as soft spheres, and their excluded volume is accounted for by the Weeks−Chandler−Anderson (WCA) potential:[56]

$$U_{WCA}(r_{ij}) = \begin{cases} 4\varepsilon\left[\left(\frac{\sigma}{r_{ij}}\right)^{12} - \left(\frac{\sigma}{r_{ij}}\right)^{6} + \frac{1}{4}\right] & \text{if } r_{ij} < r_{cut} \\ 0 & \text{otherwise} \end{cases} \quad (2)$$

where r_{ij} is the distance between two interacting particle i and j and $r_{cut} = 2^{1/6}\sigma$ is the cutoff radius.

Electrostatic interactions are calculated via the P^{3}M method, with an accuracy set to 10^{-3}. The solvent, whose molecular structure is neglected, is accounted for by a uniform dielectric continuum with a tunable Bjerrum length, l_B.

Simulation Protocol. The system is evolved with Langevin dynamics simulations

$$m_i\ddot{\mathbf{r}}_i = -\gamma\dot{\mathbf{r}}_i + \mathbf{F}_i + \mathbf{R}_i \quad (3)$$

where m_i, $\dot{\mathbf{r}}_i$, and $\ddot{\mathbf{r}}_i$ are respectively the mass, velocity, and acceleration of the ith particle, $\gamma = \sigma^{-1}/(m\varepsilon)^{1/2}$, and $\mathbf{F}_i$, and $\mathbf{R}_i$ are respectively the conservative and the random forces acting on particle i. Random forces act on each particle independently and obey the fluctuation−dissipation theorem.

All simulations were performed with the software package ESPResSo 4.1,[57] using default values for particles' mass, m, and friction coefficient, γ. The stochastic dynamics was integrated with a velocity-Verlet algorithm using a time step $\delta t = 0.01\tau_{MD}$, with $\tau_{MD} = \sigma\sqrt{(m/\varepsilon)}$.

For each considered condition, we collected at least 30 independent trajectories, each of duration $t_{sim} = 2 \times 10^4\tau_{MD}$, after an initial relaxation stage of duration $t_{therm} = 5 \times 10^3\tau_{MD}$. Canonical expectation values of the system properties were computed over system configurations sampled at intervals of $10\tau_{MD}$.

Conformational and Thermodynamical Analysis. To characterize the size of the coPE, its dependence on the composition (i.e., the NS length versus N_{neu}), and the solution properties, we considered the radius of gyration

$$R_g^{\ 2} = \sum_{i=1}^{N_{mono}} \frac{(\mathbf{r}_{CoM} - \mathbf{r}_i)^2}{N_{mono}} \quad (4)$$

where $\mathbf{r}_i$ and $\mathbf{r}_{CoM}$ are the coordinate vectors of respectively the ith monomer and center of mass of the coPE.

The analysis of the knot size was performed with the KymoKnot software package, adopting a bottom-up search algorithm.[58,59] Differently from the definition of the knotted state of an entire ring, which is a well-defined topological property, measuring the knot length requires to choose a closure scheme to assign a topological state to various portions (open arcs) of the ring. Here we adopt the minimally invasive closure scheme,[58,59] which bridges the arc's termini either directly or via the convex hull, depending on the shortest route. The knotted region is then identified from combinatorial search of the smallest arc that, upon closure, yields the same topology of the entire ring. The number of monomer in the knotted region is then taken as the knot length, l_K. For convenience of discussion, we shall use the adjectives "*tight*" and "*loose*" to indicate a knot of respectively low ($\lesssim$0.25) and high l_K/N_{mono} ratio.

https://doi.org/10.1021/acs.macromol.2c01933
Macromolecules 2022, 55, 10761−10772

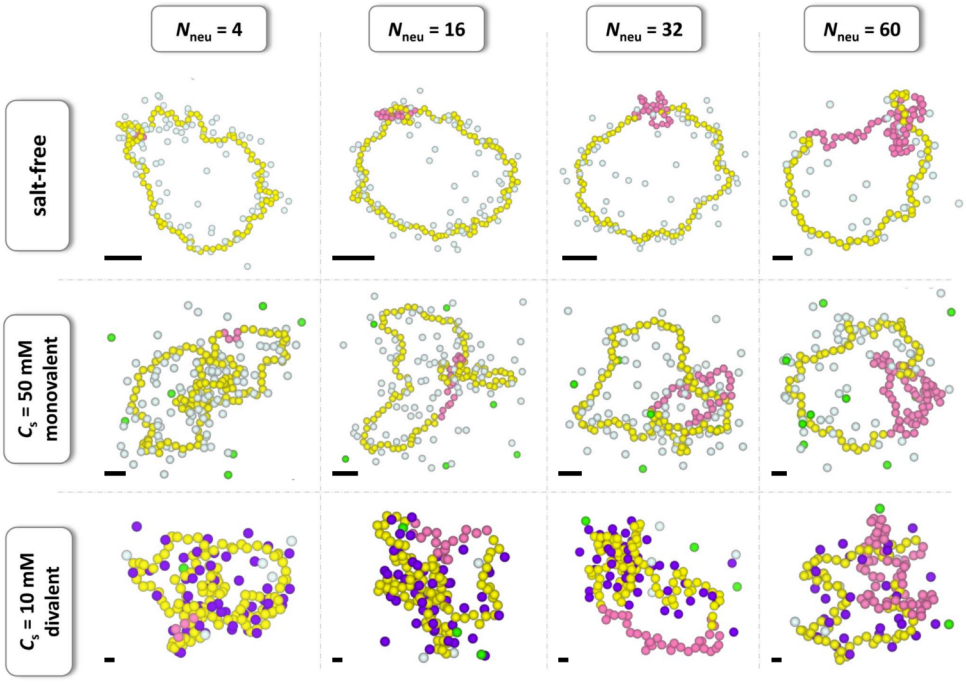

Figure 1. Trajectory snapshots for systems with various N_{neu} values and different salt conditions. Color scheme: neutral monomers in fuchsia, negatively charged monomers in yellow, coPE's counterions and monovalent salt cations in light cyan, divalent salt cations in purple, and mono- and divalent salt anions in green. For clarity, we drew only the ions close to the coPE. Because the conformations are not in scale, for each of them we have added a black bar whose length is proportional to the $\langle R_g^2 \rangle$ value.

Other salient properties that are established based on the knotted regions are (i) $\rho(\delta_{NS})$, the probability that monomer i lying at a contour distance δ_{NS} from the NS midpoint belongs to the knot;[43] (ii) $\rho_{mid}(\delta_{NS-K})$, the probability for the knot midpoint to be at distance δ_{NS-K} from the NS midpoint;[43] (iii) Φ_K, the fraction of knot occupied by the NS; (iv) Φ_{NS}, the fraction of NS occupied by the knot; and (v) p, the probability that *at least* one neutral monomer belongs to the knot (i.e., that there is some overlap between the knot and the NS). See the Supporting Information for a more detailed discussion about these properties and their calculation. Clearly, both Φ_K and Φ_{NS} represent quantitative measures of the degree of overlap between the knot region and the NS and, as such, provide indications on their relative positioning.

As for the probability p introduced in item (v), we note that its complement, $1 - p$, is the probability that *no* neutral monomers take part to the knot. Thus, the ratio $p/(1 - p)$ is related to the difference in Helmholtz energy A between two properly defined canonical macrostates, corresponding to NS being somewhat involved in or completely outside the knotted region. Accordingly, the reversible work (i.e., the change in Helmholtz energy) required to eliminate any overlap between the NS and the knot is

$$\Delta A = -k_B T \ln\left[\frac{1-p}{p}\right] \tag{5}$$

We shall use the latter equation in connection with results involving divalent salts and for varying solvent Bjerrum length. In the cases where $p \simeq 1$, $\Delta A \gg k_B T$; we shall dub the latter as "pinned" to indicate that there is always overlap between the NS and knot. Importantly, it was possible to calculate ΔA only for coPE's with short NS, as $1 - p$ values are negligible for $N_{neu} \gtrsim 32$ (*vide infra*; Figures 3c and 5c). Indeed, the computation of ΔA for the latter systems would have required rare-event sampling methods, the implementation of which was considered beyond the general aim of this study.

RESULTS

Monovalent Salts. We first discuss how knotted coPE's of different composition respond to varying amounts of monovalent (i.e., $z = 1$) background salt pairs in solution. The main structural implications are aptly conveyed by the graphical summary of Figure 1, where the two top rows present typical configurations of the knotted rings without (salt-free cases, top row) and with (C_s = 50 mM, middle row) monovalent salt. First, at each considered coPE composition, i.e., at fixed N_{neu}, the knot becomes looser with added monovalent salt pairs. Second, the knot is tightest at intermediate NS lengths ($N_{neu} \sim 16-32$), regardless of the presence of added salt. However, while in the salt-free case the knotted region tends to coincide with the NS, or even be fully contained in it, at C_s = 50 mM the knot typically extends beyond the NS, thus covering part of the charged block, too. Finally, more CI's seem to lie near the knotted region in the added salt case, especially for the smaller values of N_{neu}. A systematic analysis of these emergent properties is discussed below.

We first consider the effects of salt concentration and coPE composition on the length of the knotted region, $\langle l_K \rangle$, and the overall ring size, $\langle R_g^2 \rangle$, which are respectively presented in panels a and b of Figure 2. Consistently with earlier results for the salt-free case,[43] $\langle l_K \rangle$ versus N_{neu} curves are nonmonotonic with a single minimum at intermediate NS lengths. The new and important insight is that the nonmonotonic character of the curves in the salt-free case persists at all ionic strengths of the 1:1 salt solution. However, while the minimum in $\langle l_K \rangle$ is at N_{neu} = 16 in the salt-free case, it moves to N_{neu} = 32 when C_s =

https://doi.org/10.1021/acs.macromol.2c01933
Macromolecules 2022, 55, 10761−10772

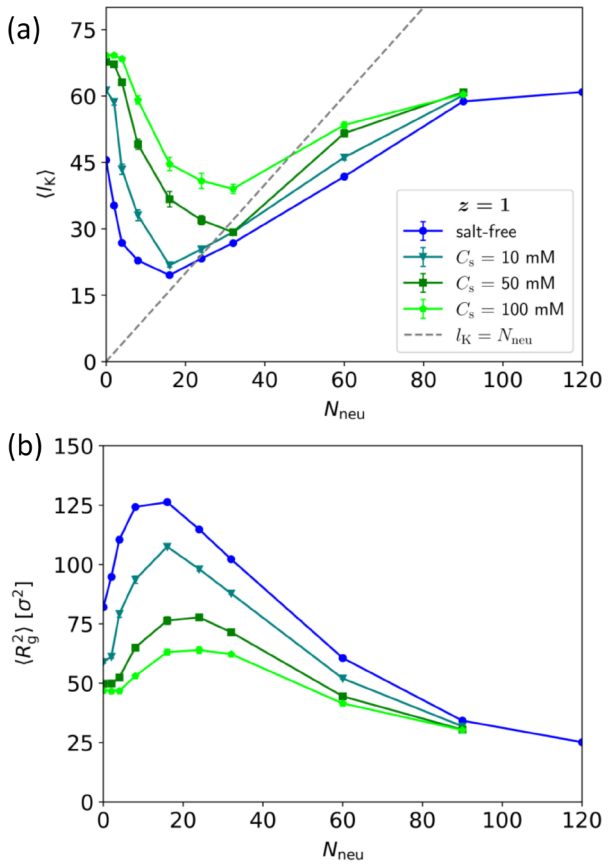

Figure 2. (a) Average knot length $\langle l_K \rangle$ and (b) average radius of gyration $\langle R_g^2 \rangle$ as a function of N_{neu} for systems with various monovalent salt concentrations C_s. In (a), the straight line $l_K = N_{neu}$ is reported as reference.

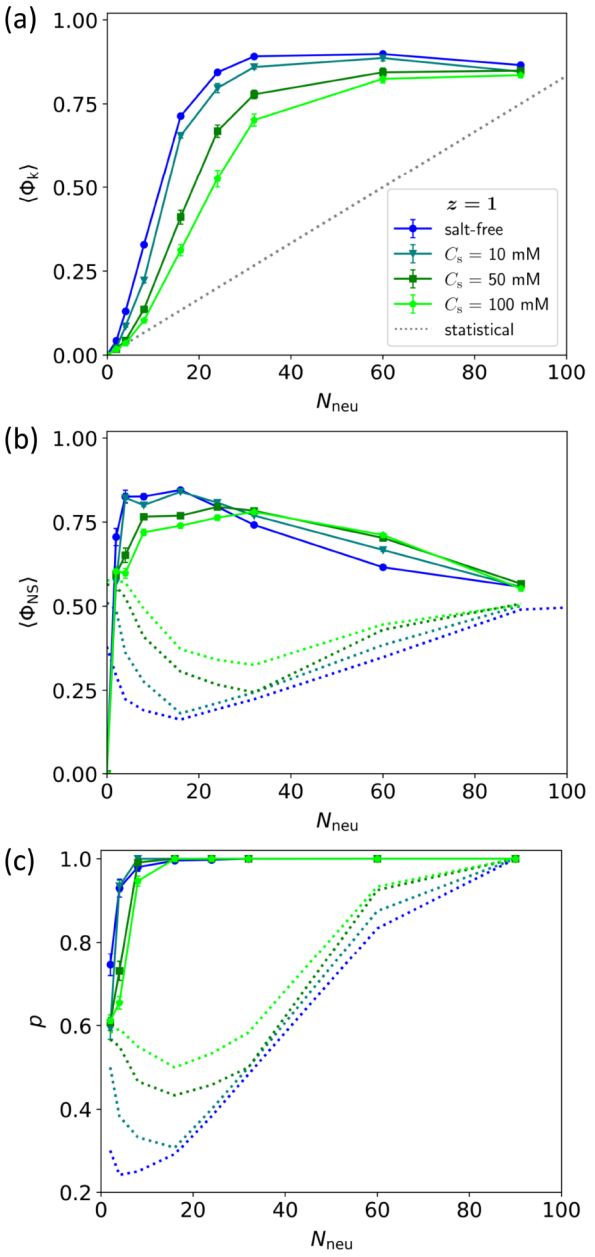

Figure 3. (a) $\langle \Phi_K \rangle$, (b) $\langle \Phi_{NS} \rangle$, and (c) probability p as a function of N_{neu} for systems with various concentrations of monovalent salts. Dotted lines represent statistical values for noninteracting systems with knot lengths equal to the $\langle l_K \rangle$ values reported in Figure 2a (see the Supporting Information for details).

50 and 100 mM. Furthermore, the entire $\langle l_K \rangle$ curves shift to higher values upon salt addition, with about a 2-fold increase from C_s = 0 to C_s = 100 mM at the tightest knot size. Analogous considerations can be made for $\langle R_g^2 \rangle$, which anticorrelates with $\langle l_K \rangle$ and systematically decreases with C_s because of the overall screening effect produced by dissolved salts (*vide infra* for further details).

The minima of $\langle l_K \rangle$ curves in Figure 2 are well aligned with the reference (dashed) line $\langle l_K \rangle = N_{neu}$, suggesting the appealing possibility that the knot in its tightest conformation mostly coincides with the NS. This idea is, however, not supported by the results of Figure 3, where the two measures of overlap between knot and NS, $\langle \Phi_K \rangle$ and $\langle \Phi_{NS} \rangle$, are shown in panels a and b, respectively. In fact, throughout the considered combinations of N_{neu} and C_s, the NS hardly spans more than 80% of the knot, and vice versa. These evidence reflect a sophisticated balance of different thermodynamic forces that define the relative positioning of the knot which minimizes the systems Helmholtz energy. On the one hand, the knot tends to occupy the NS to diminish the electrostatic repulsion of the so-called essential crossings, which are the regions kept into spatial proximity by the nontrivial topology of the ring. On the other hand, confining the entire knot in the NS is entropically costly, particularly for small NS. Consequently, part of the knot remains composed of charged beads, and part of the NS remains in the knot complementary arc. This notwithstanding, the measures of overlap, $\langle \Phi_K \rangle$ and $\langle \Phi_{NS} \rangle$, are invariably larger than the predicted for a random relative positioning of NS and a knot of length equal to $\langle l_K \rangle$.

The alternative measure of localization provided by the probability p of finding at least a NS monomer included in the knot (see Figure 3c) also supports our conclusions, with a probability to find the knot entirely contained in the charged region that is negligible for $N_{neu} \geq 8$, regardless of the amount of added salt. Furthermore, comparing the curves in Figures 2 and 3 reveals that for each salt concentrations the maximum of $\langle \Phi_{NS} \rangle$ occurs roughly at the same NS length yielding the minimum of $\langle l_K \rangle$ and the maximum of $\langle R_g^2 \rangle$. This fact can, again, be ascribed to a balance between the electrostatic repulsion of charged monomers inside and outside the knotted

https://doi.org/10.1021/acs.macromol.2c01933
Macromolecules 2022, 55, 10761−10772

region and the entropic cost of localizing the knot,[60] which can be articulated as follows:

(i) Upon increasing N_{neu}, a longer portion ($\gtrsim$70%) of the short NS is co-opted inside the knotted region to reduce the internal repulsion of knot. This can be effectively achieved by neutralizing at least one of the monomers involved in the essential crossings.[43] The latter, which are three for the 3_1 topology considered here, involve two facing strands maintained at close proximity by the topology of the ring. The partially neutral knotted region can further lower the overall intermonomer repulsion by becoming tighter than in the fully charged case, as this allows for the expansion of the complementary unknotted arc. The latter, in fact, mostly comprises charged monomers, and hence it expands, as if endowed with an effective bending rigidity.[60]

(ii) Neutralizing a single monomer in each pair defining the essential crossings already suffices to substantially lower the knot electrostatic repulsion.[43] Accordingly, it is expected that increasingly longer portions of the NS would be left in the complementary arc when N_{neu} is increased beyond the value where the NS can cover one side of three essential crossings. The consequence of this is clearly that repulsion between monomers in the complementary arc is eventually reduced by increasing N_{neu}. In turn, the knot can become looser, raising the overall entropy and, consequently, reducing $\langle R_g^2 \rangle$.

(iii) The observed mitigation of the above-mentioned effects upon increasing the concentration of weakly coordinating monovalent salt can be related to a reduced intermonomer repulsion, which decreases the effective bending rigidity of the unknotted portion of the ring.[60] This diminished rigidity, which allows for knot expansion at the expense of the unknotted arc, can thus also account for the increase of $\langle l_K \rangle$, and the accompanying decrease of $\langle R_g^2 \rangle$, with salt concentration. Finally, salt screening can weaken the repulsion of charged monomers in the vicinity of the essential crossings, where salt cations have tendency to condense. This effect helps to rationalize the diminishing overlap between knot and NS with salt concentration demonstrated by the $\langle \Phi_K \rangle$ and $\langle \Phi_{NS} \rangle$ curves, as the increased screening compensates for the repulsion between (charged) monomers at essential crossings not covered by the NS.

Divalent Salts. We observe several major changes in the knotted coPE properties upon switching from monovalent to divalent salts. As evident from the schematic overview of Figure 1 (bottom row), adding divalent salt pairs compacts the coPE and, concurrently, promotes an increase in length of the knot, which significantly spreads over the charged block when $N_{neu} \leq 32$.

The overall size reduction of the coPE ring with 2:2 salts is a consequence of charged portions of the rings lumping together around divalent cations, similar to what was previously reported for other polyelectrolyte systems and divalent CI's.[45,47−50,52−54] The loosening of the knot and its sizable footprint on the charged block have, instead, no analogues with previous results for knotted coPE's in the salt-free case; they also starkly differ from results discussed above for monovalent salts, where a substantial overlap of the knot and NS is necessary to minimize the systems' Helmholtz energy.

For a systematic analysis of the differences from the $z = 1$ case, we first present in Figure 4 the behavior of $\langle l_K \rangle$ (panel a)

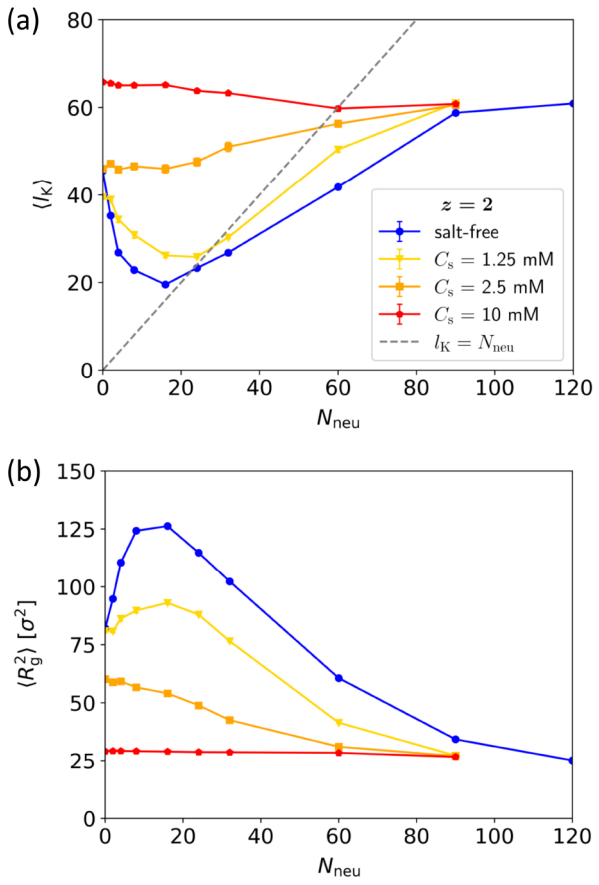

Figure 4. (a) Average knot length $\langle l_K \rangle$ and (b) average radius of gyration $\langle R_g^2 \rangle$ as a function of N_{neu} for systems with various divalent salt concentrations C_s. In (a), the straight line $l_K = N_{neu}$ is reported as reference.

and $\langle R_g^2 \rangle$ (panel b) as a function of N_{neu} and for various divalent salt concentrations. The accompanying probability distributions for l_K and R_g^2 are provided in Figures S5 and S6. Unlike the monovalent case, neither $\langle R_g^2 \rangle$ nor $\langle l_K \rangle$ shows the previously evidenced nonmonotonic behavior if a sufficiently large divalent salt concentration (i.e., $C_s \geq 2.5$) is present. In fact, the $\langle R_g^2 \rangle$ curves agree rather well with previous findings for the titration of 3_1 knotted weak polyelectrolyte rings in the presence of divalent salt,[45] whose results indicated an increase of $\langle R_g^2 \rangle$ with the polyelectrolyte ionization degree when C_s = 2.5 mM, while the ring size only marginally increased when C_s = 10 mM. In both cases, the multidentate coordination of divalent cations, especially involving distant charged chain segments, was the root cause of the discussed behavior. Besides, the vast majority of monovalent (cationic) CI's "evaporates" due to the repulsion with divalent ones,[45,61,62] thus partially compensating for the loss of entropy of the latter and of the coPE.

Taking all the above into account, the $\langle R_g^2 \rangle$ and $\langle l_K \rangle$ trends of Figure 4 can be rationalized as follows:

(i) The concentration of divalent CI's may not be sufficient to cause the complete compaction of rings due to coordination when $N_{neu} = 0$ and $C_s \lesssim 2.5$ mM, as the total charge provided by divalent cations at $C_s = 2.5$ mM

https://doi.org/10.1021/acs.macromol.2c01933
Macromolecules 2022, 55, 10761−10772

is, at most, half of the ring charge. However, the effective charge of the ring, and its self-repulsion, too, decrease with N_{neu}. Thus, the impact on the conformational property of the divalent cation coordination becomes progressively more evident, leading to a decrease in ring size (see Figures S6 and S7).

(ii) As divalent cations provide twice the total monomer charge when $N_{neu} = 0$ and $C_s = 10$ mM, there is a sufficiently high number of the former to cause ring compaction. In this situation, the increase of N_{neu} should not be expected to induce any important change in the values of $\langle R_g^2 \rangle$ and $\langle l_K \rangle$, as it would only partially weaken monomer repulsion.

The overlap between the knot and NS is also significantly different from the monovalent case, as shown by $\langle \Phi_K \rangle$ and $\langle \Phi_{NS} \rangle$ (see respectively Figures 5a and 5b). The observed trends, and their differences with respect to the $z = 1$ case, can be rationalized with the notion that divalent cations coordinate on the charged portion of the knotted ring; this can make energetically more advantageous for the rings to bring charged monomers closer as C_s is increased. With these premises, it appears plausible that the overlap between knot and NS may not be as crucial as in the monovalent case for minimizing the Helmholtz energy. This is supported by the fact that p (Figure 5c), $\langle \Phi_K \rangle$, and $\langle \Phi_{NS} \rangle$ are close to, or even fall below, those of the null statistical model at $C_s = 10$ mM. The result suggests that the overlap between knot and NS is not advantageous and that the energy gain from divalent cations coordination can compensate for the increased repulsive energy due to the higher charge density in the knotted region. Indeed, high concentrations of divalent ions can even promote the preferential overlap of the NS with the unknotted region, as shown in Figures S8 and S9.

An energy-based standpoint can substantiate the observed changes with increasing concentration of divalent salts. To this end, we harnessed the p values of Figure 5c to compute the reversible work required to eliminate the overlap between NS and knot, ΔA, at different divalent salt concentrations (see eq 5). The results as shown in Figure 6 indicate that, as expected, ΔA increases monotonically with the NS length in all conditions. A similar behavior is also found in the presence of monovalent salts (see Figure S4), although in such case the observed differences are not robust from a statistical point of view. In spite of such common traits, ΔA is markedly lower than the salt-free case when $C_s = 2.5$ and 10 mM, the cases $C_s = 0$ and 1.25 mM being substantially indistinguishable from the statistical point of view. As an example, we notice that the reversible work needed to unpin the knot in a coPE with, e.g., $N_{neu} = 16$ decreases by ~2.5 and ~6 k_BT units in the presence of a divalent salt with concentration $C_s = 2.5$ and 10 mM, respectively.

Solvent Bjerrum Length. As the salt ions' coordination appears to strongly influence the conformations of knotted coPE's, it is interesting to evaluate how varying the solvent screening power may also impact the coPE's through the modifications of the relative spatial distribution of monomers and freely moving ions. Thus, we performed a series of simulations where we exclusively considered the monovalent coPE's counterions (hence, $C_s = 0$) and varied the solvent screening power by changing the system Bjerrum length, $l_B = e^2/(4\pi\varepsilon_0\varepsilon_r k_B T)$, where e is the elementary charge, ε_0 is the vacuum dielectric constant, and ε_r is the relative solvent

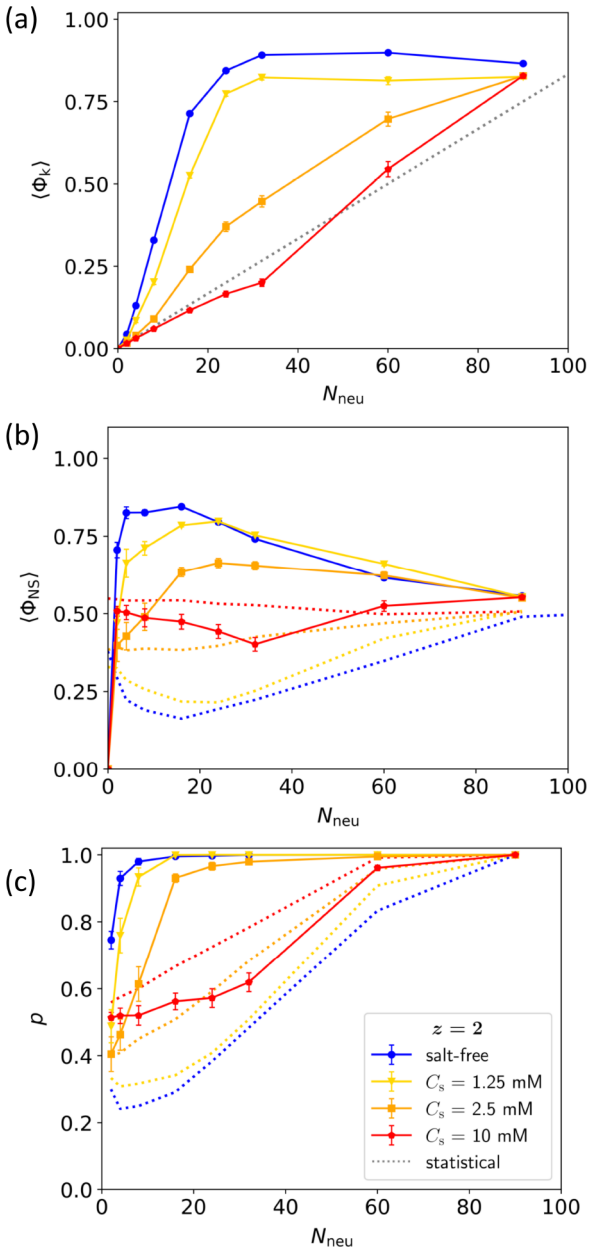

Figure 5. (a) $\langle \Phi_K \rangle$, (b) $\langle \Phi_{NS} \rangle$, and (c) probability p as a function of N_{neu} for systems with various concentrations of divalent salts. Dotted lines represent statistical values for noninteracting systems with knot lengths equal to the $\langle l_K \rangle$ values reported in Figure 4a (see the Supporting Information for details).

permittivity. We recall that in all the simulations discussed so far σ and l_B were respectively set to 3.55 Å and $2\sigma = 7.1$ Å, de facto corresponding to $\epsilon_r \approx 78$; i.e., the solvent was pure water at room temperature. Simulating systems with increased l_B may be of physicochemical relevance due to the fact that $l_B/\sigma = 3$, 4, 5, and 6 correspond to solvent relative dielectric constants $\varepsilon_r \simeq$ 53, 40, 31, and 26, which are typical values for commonly employed organic solvents. The $l_B = \sigma$ case, which corresponds to $\varepsilon_r \simeq 158$, is additionally included to gain physical insights for both the $l_B \to 0$ and $l_B \to \infty$ limits, despite the fact that solvent with such high screening power (e.g., HCN[63]) are hardly used.

To start our discussion, we focus on the impact of decreasing the solvent screening power ($l_B/\sigma = 3$, 4, 5 and

https://doi.org/10.1021/acs.macromol.2c01933
Macromolecules 2022, 55, 10761−10772

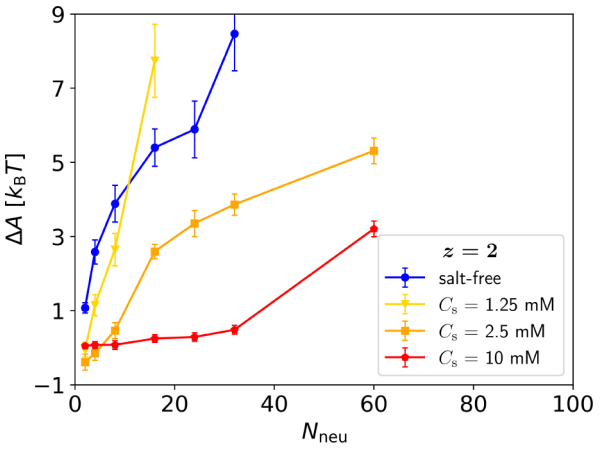

Figure 6. Difference in Helmholtz energy ΔA between pinned and unpinned conformations in various divalent salt conditions.

6) and provide a schematic summary of the findings in Figure 7, which shows typical configurations sampled during the simulations for systems with different N_{neu} and l_B values. From these, the conformational changes induced upon increasing l_B appear approximately similar to those observed upon divalent salt addition, especially regarding the number of CI's condensing on the charged portion of the coPE. The effects are quantified in Figures 8a and 8b, which present $\langle l_K \rangle$ and $\langle R_g^2 \rangle$, respectively. We observe that $\langle l_K \rangle$ curves shift to higher values as l_B increases; concomitantly, the minimum shifts to higher N_{neu} values, and the degree of nonmonotonicity decreases. In the end, $\langle l_K \rangle$ and $\langle R_g^2 \rangle$ appear to change according to a mechanism involving a reduced monomer repulsion due to an increase in CI's condensation upon increasing l_B.[45] Similarly to the cases in which salt is added, this is expected to foster the decrease in the size of the coPE, the increase in $\langle l_K \rangle$ due to a lower effective rigidity, or persistence length, in the knot complementary arc, and to diminish the importance of positioning the NS in proximity of the essential crossings or even inside the knot region.

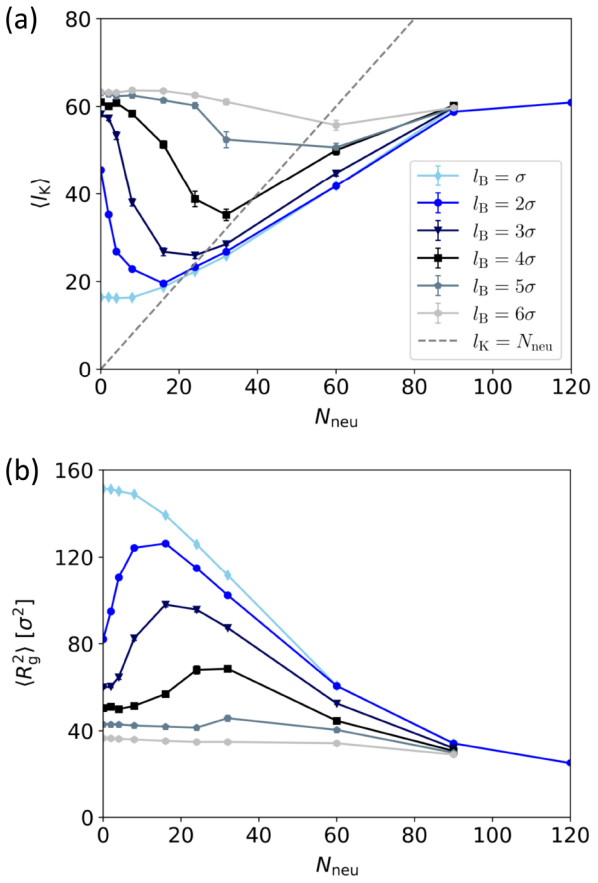

Figure 8. (a) Average knot length $\langle l_K \rangle$ and (b) average radius of gyration $\langle R_g^2 \rangle$ as a function of N_{neu} for systems with various Bjerrum lengths l_B. In (a), the straight line $l_K = N_{neu}$ is reported as reference.

What was discussed above is confirmed by the $\langle \Phi_K \rangle$, $\langle \Phi_{NS} \rangle$, and p data in Figures 9a–c. In fact, increasing l_B leads to a reduction of the overlap between knot and NS and of the probability p. Notably, p and $\langle \Phi_{NS} \rangle$ are nonmonotonic with

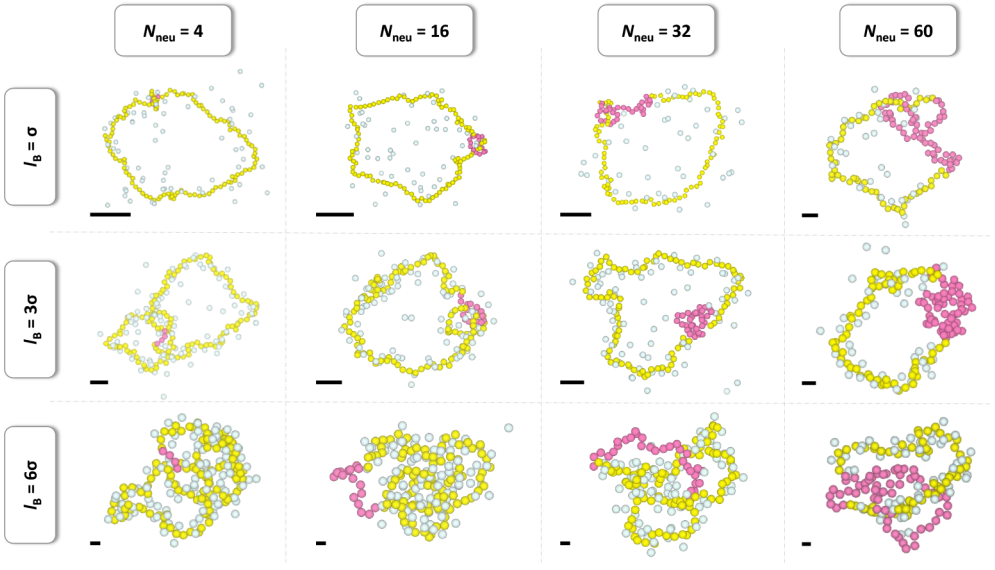

Figure 7. Trajectory snapshots for systems with various l_B and N_{neu} values. Color scheme: neutral monomers in fuchsia, negatively charged monomers in yellow, and coPE's (monovalent) counterions in light cyan. For sake of clarity, we drew only the ions close to the coPE. Because the conformations are not in scale, for each of them we have added a black bar whose length is proportional to the $\langle R_g^2 \rangle$ value.

https://doi.org/10.1021/acs.macromol.2c01933
Macromolecules 2022, 55, 10761–10772

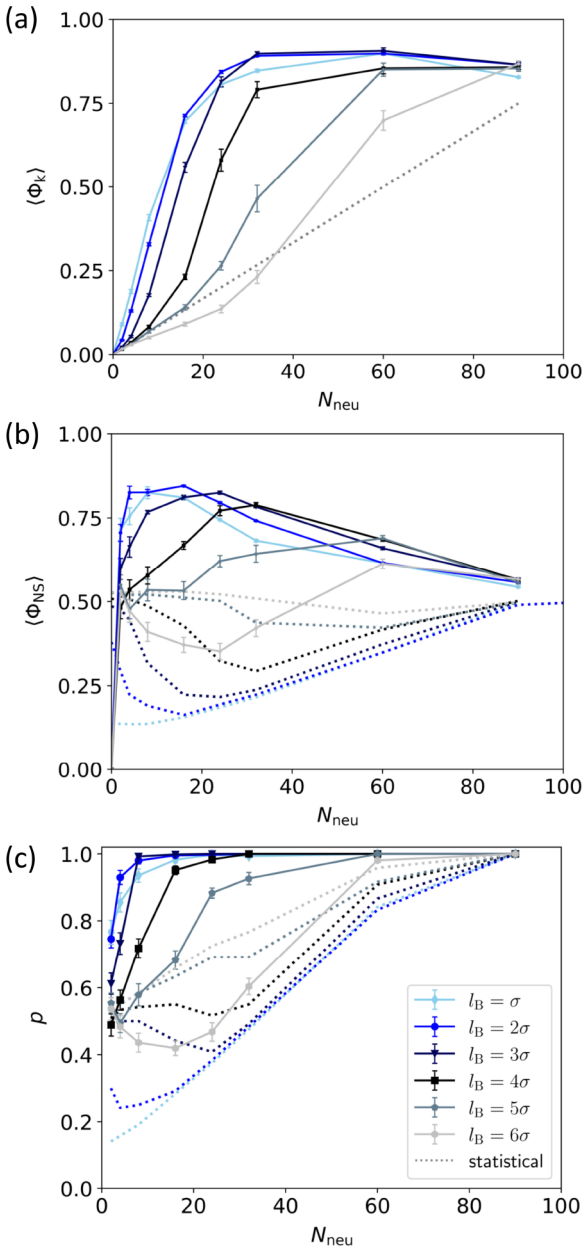

Figure 9. (a) $\langle\Phi_K\rangle$, (b) $\langle\Phi_{NS}\rangle$, and (c) probability p, as a function of N_{neu} for systems with various l_B. Dotted lines represent statistical values for noninteracting systems with knot lengths equal to the $\langle l_K\rangle$ values reported in Figure 8a (see the Supporting Information for details).

respect to N_{neu} when $l_B = 6\sigma$, a *unicum* among the cases analyzed. These observations may be explained by the diminishing energy gain afforded by including the NS in the knotted region when l_B is increased. It appears advantageous for the system to progressively push the longer NS to the knot periphery as a way of strengthening the interaction with the elevated number of condensed CI's. This conclusion is supported by the distributions $\rho(\delta_{NS})$ and $\rho_{mid}(\delta_{NS-K})$ shown respectively in Figures S11 and S12. From these, one can observe that ρ flattens as l_B increases, the distribution showing slightly higher values in the charged region for $l_B = 6\sigma$ and $8 \leq N_{neu} \leq 32$. Concomitantly, ρ_{mid} flattens as well, and its peak shifts to higher δ_{NS} values. Finally, we observe in Figure 10 that ΔA decreases upon increasing l_B, as expected. Worth

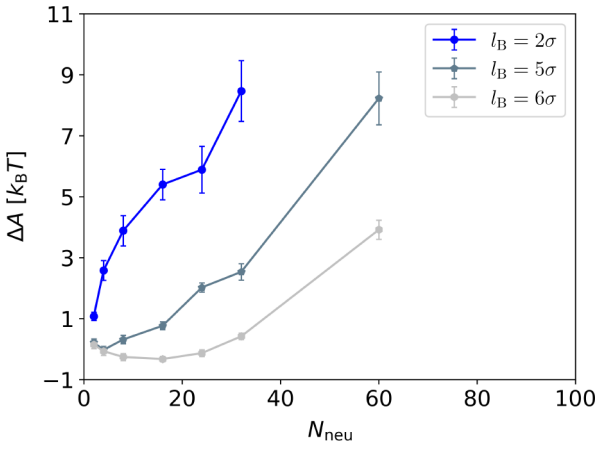

Figure 10. Difference in Helmholtz energy ΔA between pinned and unpinned conformations for systems with various l_B.

noticing, ΔA versus N_{neu} is nonmonotonic when $l_B = 6\sigma$, the unpinning process being favored by ~5.5 k_BT with respect to the $l_B = 2\sigma$ case.

To recapitulate, we present a summary of the effects of increasing solvent screening power respect to the one of water at room temperature ($l_B = \sigma$; see the trajectory snapshots provided in the first line of Figure 7). We observe qualitative deviations from the cases discussed earlier, the $\langle l_K\rangle$ and $\langle R_g^2\rangle$ curves (see Figure 8) being monotonic as a function of N_{neu}. Given the fact that $N_{neu} = 0$ corresponds to minimum in $\langle l_K\rangle$ and a maximum in $\langle R_g^2\rangle$, the results can be rationalized by noticing that the higher screening power of the solvent fosters a reduction of the number of condensed CI's (see the first row of Figure 7), which, in turn, leads to a relative increase in the repulsion between the monomers in the knot complementary arc compared to those in the knot.[45,64] As a consequence, $\langle R_g^2\rangle$ is increased and $\langle l_K\rangle$ decreased compared to the $l_B = 2\sigma$ case. Obviously, increasing N_{neu} decreases the electrostatic repulsion, which in turn reduces the size and effective persistence length of the ring.

It is instead unexpected that the probability p to find the knot on the NS decreases with respect to the $l_B = 2\sigma$ case for systems with $N_{neu} < 16$ and $l_B = \sigma$ (see Figure 8a). Indeed, we found trajectories in which a tight knot is formed on the charged block and away from the NS, the knot not being able to diffuse along the ring contour due to the significant effective persistence length. This is supported by the probability densities ρ and ρ_{mid} shown in Figure S11 for the $N_{neu} = 2$, 4, and 8 cases, in which we observe a nonzero probability in the region opposite to the NS. From such distributions it is also possible to notice a marked shoulder protruding from the neutral portion to the charged one (whereas ρ_{mid} has its peaks just outside the NS; see Figure S12), meaning that a short NS positions itself at the knot boundaries to maximize the number of essential crossings in which neutral beads are involved.[43]

SUMMARY AND CONCLUSIONS

In this work, we investigated how the solvent screening power and the solution ionic strength impact on the thermodynamical behavior of a knotted diblock copolyelectrolyte (coPE) ring composed by a neutral and a charged block of tunable lengths. For this task, we used Langevin dynamics and a coarse-grained primitive model of electrolytes.

https://doi.org/10.1021/acs.macromol.2c01933
Macromolecules 2022, 55, 10761−10772

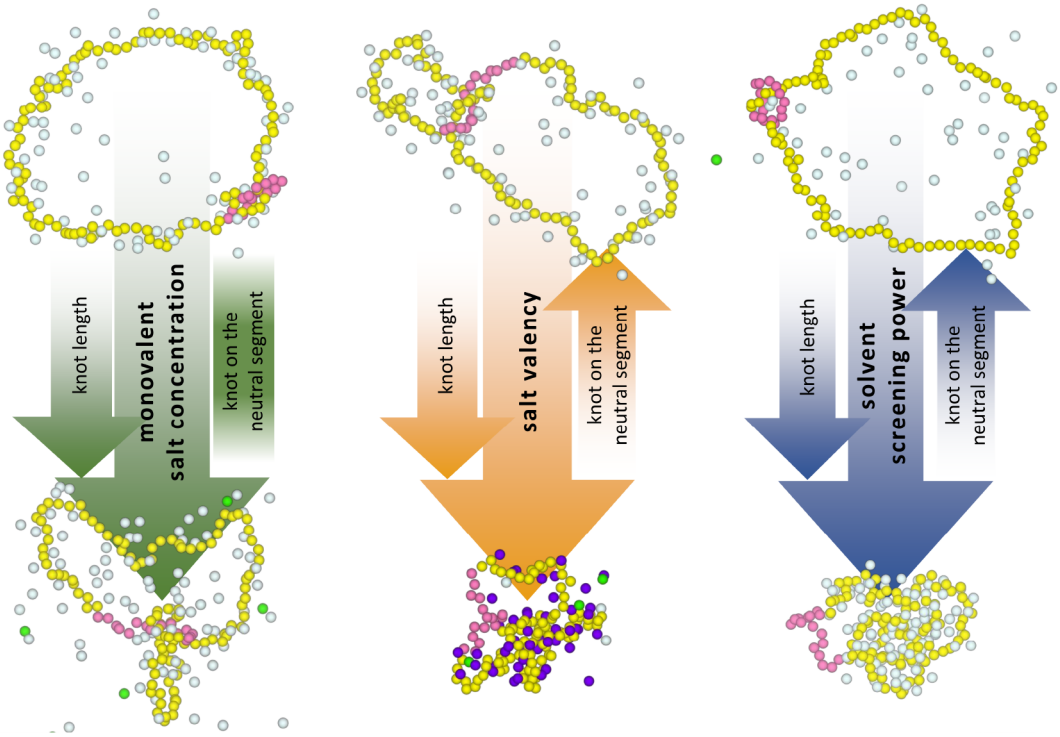

Figure 11. Scheme summarizing the conformational behavior of a coPE with N_{neu} = 16 in solution with different background ionic strength and solvent screening power. The color scheme of the coPE conformations is the same as in Figure 1. Each arrow indicates the sense in which the labeled property increases.

As for monovalent salts, we showed that the average knot length $\langle l_K \rangle$ of the coPE increases, and, consequently, the radius of gyration $\langle R_g^2 \rangle$ decreases, upon salt addition (see Figure 2). The nonmonotonic behavior of $\langle l_K \rangle$ (and $\langle R_g^2 \rangle$) observed in the salt-free case is, however, maintained, with minima (and maxima) shifted to higher N_{neu} values. Moreover, even at the largest considered concentrations, the knot conserves a large overlap with the NS, with a negligible probability to find it lying entirely on the charged block for $N_{neu} \geq 16$ (see Figure 3c).

Because of their capability of coordinating both vicinal and distant monomers when adsorbed, divalent CI's induce, instead, marked changes in the behavior of our systems, causing the collapse of the charged block (see Figure 4) and, concurrently, promoting a decrease in the knot−NS overlap when $N_{neu} \leq 32$ (see Figure 5). Besides, $\langle l_K \rangle$ and $\langle R_g^2 \rangle$ lose their nonmonotonicity already at low concentration of divalent salts, the presence of divalent CI's adsorbed along the chain making the positioning of the knot on the NS less beneficial and the knot migration on the charged portion more advantageous. Our calculations predict that the work needed to unpin the knot from the NS decreases by roughly 6 k_BT (~3.5 kcal/mol at room temperature) when C_s = 10 mM with respect to the salt-free case.

Finally, we investigated how solvent screening power impacts the structural properties of the coPE by varying the system Bjerrum length l_B (hence, the dielectric permittivity of the solvent). With respect to the reference case $l_B = 2\sigma$ (i.e., dilute aqueous solution at room temperature), increasing l_B favors CI's condensation (see Figure 7 and ref 45) fostering a marked increase in $\langle l_K \rangle$, a consequent decrease in $\langle R_g^2 \rangle$, and a reduction of the amount of reversible work needed to displace the knot from the NS (see Figures 8 and 9). Differently, solvents with lower l_B than water ought to be expected to favor knot tightening and pinning on the NS (see Figures 8 and 9). In spite of this, conformations with a tight knot on the charged segment could also be found as metastable features due to the large effective persistence length in the unscreened complementary arc.

In conclusion, we demonstrated that the presence of a knot affords much latitude for controlling the size of the coPE by solely varying the properties of the ionic solution, as summarized in Figure 11 for a coPE with N_{neu} = 16. The coPE, as we have shown, can regulate the balance of electrostatic interactions and conformational entropy of the knotted and unknotted regions, which, in turn, have direct bearings on the gyration radius of the chain. We note that though this study was performed for a fixed number of monomers, N_{mono} = 120, the results are expected to be robust for varying chain length. In fact, we explicitly verified that halving or doubling the chain length preserves the competition of electrostatics and entropy that underpins all tunable properties, including the nonmonotonicity of $\langle l_K \rangle$ and $\langle R_g^2 \rangle$. The results are presented in Figure S13, and being based on simulations without added salt, they reinforce the results of conclusions of ref 43 in addition to those of this study. In fact, the qualitative impact of salts (or l_B) is expected to be maintained, as it is solely based on the change in the relative intensities of the three major thermodynamic driving forces (see the Introduction) induced by varying the environmental properties.

Our findings complement earlier studies where metric and dynamical properties of knotted coPE's were modulated with suitable choices of coPE composition, i.e., the length of two blocks.[43] While the coPE composition cannot be altered in a facile way, salt concentration, valency, and solvent screening

https://doi.org/10.1021/acs.macromol.2c01933
Macromolecules 2022, 55, 10761−10772

power are all easily varied extrinsic parameters. Our results thus demonstrate the feasibility of achieving a facile control over coPE conformations by harnessing topology and solvent-mediated electrostatic interactions.

Our results pave the way toward attaining a broader and finer external tunability of polymer properties by considering additional solvent- or solution-dependent features as well as the overall chain length. The latter may include the degree of solvophilicity of monomers belonging to different blocks or the presence of chemical specific interactions between monomers[65−68] or with mobile ions.[69,70] For instance, a lower solvophilicity of short alternating blocks, or strong hydrogen bonding, may pin one or more essential crossings,[71] thus impacting the contour mobility of the knot.[72] An alternative way to achieve such effect would be to confer weak acid and basic properties to different chain segments, obtaining polyampholytes with switchable (e.g., by means of pH stimuli) interblock interactions and possibly different effective block rigidities.[73] The latter systems may be somewhat exploited to gain deeper physical insights into the impact of nontrivial topologies in more complicate biomacromolecules such as intrinsically disordered proteins.

Finally, because the considered systems offer multiple ways of controlling the contour positioning and spacing of the essential crossings, they represent an ideal context for systematic investigations of effective interactions of multiple knots on the same polymer chain.[74]

■ ASSOCIATED CONTENT

Supporting Information

The Supporting Information is available free of charge at https://pubs.acs.org/doi/10.1021/acs.macromol.2c01933.

Additional methodological details; additional results including l_K and R_g^2 distributions; probability densities describing the relative position between the knot and the NS; $\langle l_K \rangle$ for systems with different N_{mono} values in salt-free conditions and l_B = 2 (PDF)

■ AUTHOR INFORMATION

Corresponding Authors

Cristian Micheletti − *SISSA (Scuola Internazionale Superiore di Studi Avanzati), 34136 Trieste, Italy;* orcid.org/0000-0002-1022-1638; Email: cristian.micheletti@sissa.it

Massimo Mella − *Dipartimento di Scienza ed Alta Tecnologia, Università degli Studi dell'Insubria, 22100 Como, Italy;* orcid.org/0000-0001-7227-9715; Email: massimo.mella@uninsubria.it

Author

Andrea Tagliabue − *Dipartimento di Scienza ed Alta Tecnologia, Università degli Studi dell'Insubria, 22100 Como, Italy; SISSA (Scuola Internazionale Superiore di Studi Avanzati), 34136 Trieste, Italy;* orcid.org/0000-0001-9520-0627

Complete contact information is available at: https://pubs.acs.org/10.1021/acs.macromol.2c01933

Author Contributions

AT: ideation, software, simulation, analysis, writing, visualization. CM: supervision, analysis, writing. MM: supervision, analysis, writing, funding.

Notes

The authors declare no competing financial interest.

■ ACKNOWLEDGMENTS

M.M. acknowledges support from the Università degli Studi dell'Insubria for funding under the scheme Fondo di Ateneo per la Ricerca (FAR 2021).

■ REFERENCES

(1) Rybenkov, V. V.; Cozzarelli, N. R.; Vologodskii, A. V. Probability of DNA Knotting and the Effective Diameter of the DNA Double Helix. *Proc. Natl. Acad. Sci. U. S. A.* **1993**, *90*, 5307−5311.

(2) Seeman, N. C. Nucleic Acid Nanostructures and Topology. *Angew. Chem., Int. Ed.* **1998**, *37*, 3220−3238.

(3) Arsuaga, J.; Vázquez, M.; Trigueros, S.; Sumners, D. W.; Roca, J. Knotting Probability of DNA Molecules Confined in Restricted Volumes: DNA Knotting in Phage Capsids. *Proc. Natl. Acad. Sci. U. S. A.* **2002**, *99*, 5373−5377.

(4) Micheletti, C.; Marenduzzo, D.; Orlandini, E. Polymers with Spatial or Topological Constraints: Theoretical and Computational Results. *Phys. Rep.* **2011**, *504*, 1−73.

(5) Tang, J.; Du, N.; Doyle, P. S. Compression and Self-Entanglement of Single DNA Molecules Under Uniform Electric Field. *Proc. Natl. Acad. Sci. U. S. A.* **2011**, *108*, 16153−16158.

(6) Klotz, A. R.; Narsimhan, V.; Soh, B. W.; Doyle, P. S. Dynamics of DNA Knots During Chain Relaxation. *Macromolecules* **2017**, *50*, 4074−4082.

(7) Valdés, A.; Coronel, L.; Martínez-García, B.; Segura, J.; Dyson, S.; Díaz-Ingelmo, O.; Micheletti, C.; Roca, J. Transcriptional Supercoiling Boosts Topoisomerase II-Mediated Knotting of Intracellular DNA. *Nucleic Acids Res.* **2019**, *47*, 6946−6955.

(8) Potestio, R.; Micheletti, C.; Orland, H. Knotted vs. Unknotted Proteins: Evidence of Knot-Promoting Loops. *PLoS computational biology* **2010**, *6*, No. e1000864.

(9) Virnau, P.; Mallam, A.; Jackson, S. Structures and Folding Pathways of Topologically Knotted Proteins. *J. Phys.: Condens. Matter* **2011**, *23*, 033101.

(10) Meluzzi, D.; Smith, D. E.; Arya, G. Biophysics of Knotting. *Annual Review of Biophysics* **2010**, *39*, 349−366.

(11) Jackson, S. E.; Suma, A.; Micheletti, C. How to Fold Intricately: Using Theory and Experiments to Unravel the Properties of Knotted Proteins. *Curr. Opin. Struct. Biol.* **2017**, *42*, 6−14.

(12) Jarmolinska, A. I.; Perlinska, A. P.; Runkel, R.; Trefz, B.; Ginn, H. M.; Virnau, P.; Sulkowska, J. I. Proteins' Knotty Problems. *J. Mol. Biol.* **2019**, *431*, 244−257.

(13) Ayme, J.-F.; Beves, J. E.; Campbell, C. J.; Leigh, D. A. Template Synthesis of Molecular Knots. *Chem. Soc. Rev.* **2013**, *42*, 1700−1712.

(14) Fielden, S. D.; Leigh, D. A.; Woltering, S. L. Molecular Knots. *Angew. Chem., Int. Ed.* **2017**, *56*, 11166−11194.

(15) Marenda, M.; Orlandini, E.; Micheletti, C. Discovering Privileged Topologies of Molecular Knots with Self-Assembling Models. *Nat. Commun.* **2018**, *9*, 1−8.

(16) Grosberg, A.; Rabin, Y.; Havlin, S.; Neer, A. Crumpled Globule Model of the Three-Dimensional Structure of DNA. *EPL (Europhysics Letters)* **1993**, *23*, 373.

(17) Virnau, P.; Kantor, Y.; Kardar, M. Knots in Globule and Coil Phases of a Model Polyethylene. *J. Am. Chem. Soc.* **2005**, *127*, 15102−15106.

(18) Ercolini, E.; Valle, F.; Adamcik, J.; Witz, G.; Metzler, R.; De Los Rios, P.; Roca, J.; Dietler, G. Fractal Dimension and Localization of DNA Knots. *Physical review letters* **2007**, *98*, 058102.

(19) Deguchi, T.; Uehara, E. Statistical and Dynamical Properties of Topological Polymers with Graphs and Ring Polymers with Knots. *Polymers* **2017**, *9*, 252.

(20) Amici, G.; Caraglio, M.; Orlandini, E.; Micheletti, C. Topologically Linked Chains in Confinement. *ACS Macro Lett.* **2019**, *8*, 442−446.

(21) Zhang, J.; Meyer, H.; Virnau, P.; Daoulas, K. C. Can Soft Models Describe Polymer Knots? *Macromolecules* **2020**, *53*, 10475−10486.
(22) Grosberg, A. Y.; Nechaev, S. K.; Shakhnovich, E. I. The Role of Topological Constraints in the Kinetics of Collapse of Macromolecules. *Journal de physique* **1988**, *49*, 2095−2100.
(23) Everaers, R.; Sukumaran, S. K.; Grest, G. S.; Svaneborg, C.; Sivasubramanian, A.; Kremer, K. Rheology and Microscopic Topology of Entangled Polymeric Liquids. *Science* **2004**, *303*, 823−826.
(24) Tzoumanekas, C.; Theodorou, D. N. Topological Analysis of Linear Polymer Melts: A Statistical Approach. *Macromolecules* **2006**, *39*, 4592−4604.
(25) Rosa, A.; Everaers, R. Structure and Dynamics of Interphase Chromosomes. *PLoS Comput. Biol.* **2008**, *4*, No. e1000153.
(26) Micheletti, C.; Orlandini, E. Knotting and Unknotting Dynamics of DNA Strands in Nanochannels. *ACS Macro Lett.* **2014**, *3*, 876−880.
(27) Amin, S.; Khorshid, A.; Zeng, L.; Zimny, P.; Reisner, W. A Nanofluidic Knot Factory Based on Compression of Single DNA in Nanochannels. *Nat. Commun.* **2018**, *9*, 1−10.
(28) Michieletto, D.; Orlandini, E.; Turner, M. S.; Micheletti, C. Separation of Geometrical and Topological Entanglement in Confined Polymers Driven out of Equilibrium. *ACS Macro Lett.* **2020**, *9*, 1081−1085.
(29) Smrek, J.; Chubak, I.; Likos, C. N.; Kremer, K. Active Topological Glass. *Nat. Commun.* **2020**, *11*, 1−11.
(30) Farago, O.; Kantor, Y.; Kardar, M. Pulling Knotted Polymers. *Europhys. Lett.* **2002**, *60*, 53−59.
(31) Bao, X. R.; Lee, H. J.; Quake, S. R. Behavior of Complex Knots in Single DNA Molecules. *Physical review letters* **2003**, *91*, 265506.
(32) Huang, L.; Makarov, D. E. Langevin Dynamics Simulations of the Diffusion of Molecular Knots in Tensioned Polymer Chains. *J. Phys. Chem. A* **2007**, *111*, 10338−10344.
(33) Caraglio, M.; Micheletti, C.; Orlandini, E. Stretching Response of Knotted and Unknotted Polymer Chains. *Phys. Rev. Lett.* **2015**, *115*, 188301.
(34) Metzler, R.; Reisner, W.; Riehn, R.; Austin, R.; Tegenfeldt, J.; Sokolov, I. M. Diffusion Mechanisms of Localised Knots Along a Polymer. *EPL (Europhysics Letters)* **2006**, *76*, 696.
(35) Renner, C. B.; Doyle, P. S. Stretching Self-Entangled DNA Molecules in Elongational Fields. *Soft Matter* **2015**, *11*, 3105−3114.
(36) Liebetreu, M.; Ripoll, M.; Likos, C. N. Trefoil Knot Hydrodynamic Delocalization on Sheared Ring Polymers. *ACS Macro Lett.* **2018**, *7*, 447−452.
(37) Ma, Z.; Dorfman, K. D. Diffusion of Knots along DNA Confined in Nanochannels. *Macromolecules* **2020**, *53*, 6461−6468.
(38) Soh, B. W.; Doyle, P. S. Deformation Response of Catenated DNA Networks in a Planar Elongational Field. *ACS Macro Lett.* **2020**, *9*, 944−949.
(39) Liebetreu, M.; Likos, C. N. Hydrodynamic Inflation of Ring Polymers Under Shear. *Commun. Mater.* **2020**, *1*, 1−11.
(40) Suma, A.; Rosa, A.; Micheletti, C. Pore Translocation of Knotted Polymer Chains: How Friction Depends on Knot Complexity. *ACS Macro Lett.* **2015**, *4*, 1420−1424.
(41) Plesa, C.; Verschueren, D.; Pud, S.; Van Der Torre, J.; Ruitenberg, J. W.; Witteveen, M. J.; Jonsson, M. P.; Grosberg, A. Y.; Rabin, Y.; Dekker, C. Direct Observation of DNA Knots Using a Solid-State Nanopore. *Nat. Nanotechnol.* **2016**, *11*, 1093−1097.
(42) Caraglio, M.; Orlandini, E.; Whittington, S. G. Translocation of Links Through a Pore: Effects of Link Complexity and Size. *Journal of Statistical Mechanics: Theory and Experiment* **2020**, *2020*, 043203.
(43) Tagliabue, A.; Micheletti, C.; Mella, M. Tunable Knot Segregation in Copolyelectrolyte Rings Carrying a Neutral Segment. *ACS Macro Lett.* **2021**, *10*, 1365−1370.
(44) Orlandini, E.; Baiesi, M.; Zonta, F. How Local Flexibility Affects Knot Positioning in Ring Polymers. *Macromolecules* **2016**, *49*, 4656−4662.
(45) Tagliabue, A.; Izzo, L.; Mella, M. Interface Counterion Localization Induces a Switch between Tight and Loose Configurations of Knotted Weak Polyacid Rings despite Intermonomer Coulomb Repulsions. *J. Phys. Chem. B* **2020**, *124*, 2930−2937.
(46) Gao, X.; Xu, X. Salt Effects on Knot Dynamics in Polyelectrolyte Solutions. *Mol. Simul.* **2022**, *48*, 273−281.
(47) Liu, S.; Ghosh, K.; Muthukumar, M. Polyelectrolyte Solutions With Added Salt: A Simulation Study. *J. Chem. Phys.* **2003**, *119*, 1813−1823.
(48) Carnal, F.; Stoll, S. Chain Stiffness, Salt Valency, and Concentration Influences on Titration Curves of Polyelectrolytes: Monte Carlo Simulations. *J. Chem. Phys.* **2011**, *134*, 044909.
(49) Jusufi, A.; Borisov, O.; Ballauff, M. Structure Formation in Polyelectrolytes Induced by Multivalent Ions. *Polymer* **2013**, *54*, 2028−2035. Special issue in honor of Axel H. E. Müller.
(50) Chremos, A.; Douglas, J. F. Influence of Higher Valent Ions on Flexible Polyelectrolyte Stiffness and Counter-Ion Distribution. *J. Chem. Phys.* **2016**, *144*, 164904.
(51) Yu, J.; Mao, J.; Yuan, G.; Satija, S.; Jiang, Z.; Chen, W.; Tirrell, M. Structure of Polyelectrolyte Brushes in the Presence of Multivalent Counterions. *Macromolecules* **2016**, *49*, 5609−5617.
(52) Staňo, R.; Nová, L.; Uhlík, F.; Košovan, P. Multivalent Counterions Accumulate in Star-Like Polyelectrolytes and Collapse the Polymer in Spite of Increasing Its Ionization. *Soft Matter* **2020**, *16*, 1047−1055.
(53) Jacobs, M.; Lopez, C. G.; Dobrynin, A. V. Quantifying the Effect of Multivalent Ions in Polyelectrolyte Solutions. *Macromolecules* **2021**, *54*, 9577−9586.
(54) Lopez, C. G.; Horkay, F.; Schweins, R.; Richtering, W. Solution Properties of Polyelectrolytes with Divalent Counterions. *Macromolecules* **2021**, *54*, 10583−10593.
(55) Kremer, K.; Grest, G. S. Dynamics of Entangled Linear Polymer Melts: A Molecular-Dynamics Simulation. *J. Chem. Phys.* **1990**, *92*, 5057.
(56) Weeks, J. D.; Chandler, D.; Andersen, H. C. Role of Repulsive Forces in Determining the Equilibrium Structure of Simple Liquids. *J. Chem. Phys.* **1971**, *54*, 5237−5247.
(57) Weik, F.; Weeber, R.; Szuttor, K.; Breitsprecher, K.; de Graaf, J.; Kuron, M.; Landsgesell, J.; Menke, H.; Sean, D.; Holm, C. ESPResSo 4.0 − An Extensible Software Package for Simulating Soft Matter Systems. *Eur. Phys. J-Spec. Top.* **2019**, *227*, 1789−1816.
(58) Tubiana, L.; Orlandini, E.; Micheletti, C. Probing the Entanglement and Locating Knots in Ring Polymers: A Comparative Study of Different Arc Closure Schemes. *Prog. Theor. Phys. Suppl.* **2011**, *191*, 192−204.
(59) Tubiana, L.; Polles, G.; Orlandini, E.; Micheletti, C. KymoKnot: A Web Server and Software Package to Identify and Locate Knots in Trajectories of Linear or Circular Polymers. *Eur. Phys. J. E* **2018**, *41*, 72.
(60) Dommersnes, P. G.; Kantor, Y.; Kardar, M. Knots in Charged Polymers. *Phys. Rev. E* **2002**, *66*, 031802.
(61) Horkay, F.; Tasaki, I.; Basser, P. J. Effect of Monovalent−Divalent Cation Exchange on the Swelling of Polyacrylate Hydrogels in Physiological Salt Solutions. *Biomacromolecules* **2001**, *2*, 195−199.
(62) Kundagrami, A.; Muthukumar, M. Theory of Competitive Counterion Adsorption on Flexible Polyelectrolytes: Divalent Salts. *J. Chem. Phys.* **2008**, *128*, 244901.
(63) Wohlfahrt, C.*2 Pure Liquids: Data: Datasheet from Landolt-Börnstein - Group IV Physical Chemistry · Volume 6: "Static Dielectric Constants of Pure Liquids and Binary Liquid Mixtures"*.
(64) Nová, L.; Uhlík, F.; Košovan, P. Local pH and Effective pK_A of Weak Polyelectrolytes − Insights from Computer Simulations. *Phys. Chem. Chem. Phys.* **2017**, *19*, 14376−14387.
(65) Tagliabue, A.; Izzo, L.; Mella, M. Impact of Charge Correlation, Chain Rigidity, and Chemical Specific Interactions on the Behavior of Weak Polyelectrolytes in Solution. *J. Phys. Chem. B* **2019**, *123*, 8872−8888.
(66) Tagliabue, A.; Izzo, L.; Mella, M. Absorbed Weak Polyelectrolytes: Impact of Confinement, Topology, and Chemically Specific Interactions on Ionization, Conformation Free Energy,

Counterion Condensation, and Absorption Equilibrium. *J. Polym. Sci., Part B: Polym. Phys.* **2019**, *57*, 491−510.
(67) Mella, M.; Tagliabue, A.; Mollica, L.; Izzo, L. Monte Carlo Study of the Effects of Macroion Charge Distribution on the Ionization and Adsorption of Weak Polyelectrolytes and Concurrent Counterion Release. *J. Colloid Interface Sci.* **2020**, *560*, 667−680.
(68) Mella, M.; Tagliabue, A.; Vaghi, S.; Izzo, L. Evidences for Charged Hydrogen Bonds on Surfaces Bearing Weakly Basic Pendants: The Case of PMMA−*ran*−PDMAEMA Polymeric Films. *Colloids Surf., A* **2021**, *620*, 126525.
(69) Mella, M.; Tagliabue, A. Impact of Chemically Specific Interactions between Anions and Weak Polyacids on Chain Ionization, Conformations, and Solution Energetics. *Macromolecules* **2022**, *55*, 4533−4547.
(70) Mella, M.; Tagliabue, A.; Mollica, L.; Vaghi, S.; Izzo, L. Inducing pH Control Over the Critical Micelle Concentration of Zwitterionic Surfactants via Polyacids Adsorption: Effect of Chain Length and Structure. *J. Colloid Interface Sci.* **2022**, *606*, 1636−1651.
(71) Dai, L.; Doyle, P. S. Effects of Intrachain Interactions on the Knot Size of a Polymer. *Macromolecules* **2016**, *49*, 7581−7587.
(72) Caraglio, M.; Marcone, B.; Baldovin, F.; Orlandini, E.; Stella, A. L. Topological Disentanglement of Linear Polymers Under Tension. *Polymers* **2020**, *12*, 2580.
(73) Villani, S.; Adami, R.; Reverchon, E.; Ferretti, A.; Ponti, A.; Lepretti, M.; Caputo, I.; Izzo, L. pH-Sensitive Polymersomes: Controlling Swelling via Copolymer Structure and Chemical Composition. *J. Drug Targeting* **2017**, *25*, 899−909.
(74) Ma, Z.; Dorfman, K. D. Interactions Between Two Knots in Nanochannel-Confined DNA Molecules. *J. Chem. Phys.* **2021**, *155*, 154901.

https://doi.org/10.1021/acs.macromol.2c01933
Macromolecules 2022, 55, 10761−10772